

Estimating the spectral indices of correlated astrophysical foregrounds by a second-order statistical approach

A. Bonaldi^{1,2}, L. Bedini³, E. Salerno³, C. Baccigalupi^{4,5}, G. De Zotti^{2,4}

¹Dipartimento di Astronomia, Università di Padova, vicolo dell'Osservatorio 2, I-35122 Padova, Italy

²INAF-Osservatorio Astronomico di Padova, vicolo dell'Osservatorio 5, I-35122, Padova, Italy

³Istituto di Scienza e Tecnologie dell'Informazione, CNR, Area della ricerca di Pisa, via G. Moruzzi 1, I-56124 Pisa, Italy

⁴SISSA/ISAS, via Beirut 4, I-34014 Trieste, Italy

⁵ITA, Albert-Überle-Strasse 2, 69120 Heidelberg, Germany

Accepted 2006 August 31. Received 2006 August 31; in original form 2006 April 10

ABSTRACT

We present the first tests of a new method, the Correlated Component Analysis (CCA) based on second-order statistics, to estimate the mixing matrix, a key ingredient to separate astrophysical foregrounds superimposed to the Cosmic Microwave Background (CMB). In the present application, the mixing matrix is parameterized in terms of the spectral indices of Galactic synchrotron and thermal dust emissions, while the free-free spectral index is prescribed by basic physics, and is thus assumed to be known. We consider simulated observations of the microwave sky with angular resolution and white stationary noise at the nominal levels for the PLANCK satellite, and realistic foreground emissions, with a position dependent synchrotron spectral index. We work with two sets of PLANCK frequency channels: the low frequency set, from 30 to 143 GHz, complemented with the Haslam 408 MHz map, and the high frequency set, from 217 to 545 GHz. The concentration of intense free-free emission on the Galactic plane introduces a steep dependence of the spectral index of the global Galactic emission with Galactic latitude, close to the Galactic equator. This feature makes difficult for the CCA to recover the synchrotron spectral index in this region, given the limited angular resolution of PLANCK, especially at low frequencies. A cut of a narrow strip around the Galactic equator ($|b| < 3^\circ$), however, allows us to overcome this problem. We show that, once this strip is removed, the CCA allows an effective foreground subtraction, with residual uncertainties inducing a minor contribution to errors on the recovered CMB power spectrum.

Key words: methods: data analysis - techniques: image processing - cosmic microwave background.

1 INTRODUCTION

The Cosmic Microwave Background (CMB) is by far the most powerful cosmological probe. The power spectra of its temperature and polarization anisotropies encode detailed information on the key cosmological parameters. Tremendous experimental efforts, and especially the currently flying *Wilkinson Microwave Anisotropy Probe* (WMAP, Bennett et al. 2003a, Spergel et al. 2006) and the forthcoming PLANCK satellite (Tauber 2004; Lamarre et al. 2003; Mandolesi, Morgante, & Villa 2003) will substantially advance the sensitivity and resolution of maps of the microwave sky. Correspondingly, efficient methods to extract all the available information from the measured signal need to be implemented, exploiting the advances of the data analysis science. One of the most challenging tasks is the separation of the astrophysical components superimposed on the CMB, usually denominated “foregrounds”.

On angular scales larger than about $30'$ the dominant foregrounds in the relevant spectral region are diffuse emissions from

our own Galaxy (De Zotti et al. 1999). Synchrotron (Haslam et al. 1982) and free-free (Haffner, Reynolds, & Tufte 1999, Finkbeiner 2003) emissions dominate below $\simeq 60 - 80$ GHz (Bennett et al. 2003b), while at higher frequencies thermal dust (Schlegel, Finkbeiner, Davies 1998; Finkbeiner, Schlegel, Davies 1999) takes over. On smaller angular scales foreground fluctuations are dominated by several populations of extra-galactic sources, with different spectral behaviour: radio sources, dusty galaxies and the Sunyaev-Zel'dovich effect from galaxy clusters.

A big deal of work has been recently dedicated to develop algorithms performing component separation, based on different ideas and techniques from signal processing science. Several algorithms, referred to as “non-blind”, assume a perfect knowledge of the frequency dependence of sources. The most widely used techniques exploiting this approach are Wiener Filtering (WF; Tegmark & Efstathiou 1996; Bouchet, Prunet, & Sethi 1999) and the Maximum Entropy Method (MEM; Hobson et al. 1998; Barreiro et al. 2004; Maisinger et al. 2004; Stolyarov et al. 2005). On the

other hand, the emission spectra are generally poorly known. This fact has motivated “blind” approaches, which do not make any assumption on the spectral shape. Particularly promising are methods exploiting Independent Component Analysis (ICA) techniques (Amari & Chichocki 1998; Hyvärinen 1999), relying on the statistical independence of the different components. These methods proved to be very effective in extracting the CMB, which is independent of all other sources (Baccigalupi et al. 2000, 2004; Maino et al. 2002, 2003; Stivoli et al. 2006; Patanchon et al. 2005). However, Galactic emissions are tightly correlated to each other, so that the assumption of mutual independence breaks down. Still following the ICA approach, Belouchrani et al. (1997) dropped statistical independence for mere uncorrelation, and recovered the missing information by exploiting the physically plausible assumption of a significant spatial autocorrelation of the individual sources. Bedini et al. (2005) also exploited second-order statistics and spatial autocorrelation but, at variance with Belouchrani et al. (1997), they gave up the assumption of mutually uncorrelated sources. By exploiting a parametric knowledge of the mixing matrix, they succeeded in estimating both the mixing matrix and the relevant cross-covariances.

Here we present the first tests on this method, referred to as *correlated component analysis* (CCA), on a data set as realistic as possible. Also, we work either on the whole sky or on spherical sky patches, rather than on small plane patches as in Bedini et al. (2005).

The paper is organized as follows. In Section 2 and 3 we describe the basic aspects of CCA, and its implementation. In Section 4 we illustrate the tests on simulated skies. In Section 5 and 6 we estimate the precision of the mixing matrix and CMB power spectrum recovery. In Section 7 we draw our conclusions.

2 THE CORRELATED COMPONENT ANALYSIS (CCA)

We assume that the observed sky radiation is the superposition of N different physical processes whose spatial pattern is independent of frequency spectrum:

$$x(\mathbf{r}, \nu) = \sum_{j=1}^N s_j(\mathbf{r}) f_j(\nu). \quad (1)$$

If we have a set of equal resolution observations at M different frequencies, the observed signal can be modelled as:

$$\mathbf{x} = \mathbf{H}\mathbf{s} + \mathbf{n}, \quad (2)$$

where \mathbf{x} is the M -vector of observations, \mathbf{H} is a $M \times N$ mixing matrix, \mathbf{s} is the N -vector of sources and \mathbf{n} the M -vector of instrumental noise. The generic element of the mixing matrix is related to the source spectra, $f_c(\nu)$, and to the instrumental frequency response function, $b_d(\nu)$:

$$h_{dc} = \int f_c(\nu) b_d(\nu) d\nu. \quad (3)$$

Assuming that the source spectra are constant within the passbands, eq. (3) becomes:

$$h_{dc} = f_c(\nu_d) \int b_d(\nu) d\nu, \quad (4)$$

meaning that the element h_{dc} is proportional to the spectrum of the c -th source at the central frequency ν_d of the d -th channel. In any case, h_{dc} will be proportional to f_c at an effective frequency ν_{eff} within the d -th sensor passband, depending on both the spectrum and the frequency response (see Eriksen et al. 2006).

If both the mixing matrix \mathbf{H} and the source vector \mathbf{s} are unknown, the problem is unsolvable without additional hypotheses. The CCA method exploits information on the second order statistics of the data.

The covariance matrix of a generic signal \mathbf{X} , defined in a two dimensional space with coordinates (ξ, η) , is:

$$\mathbf{C}_x(\tau, \psi) = \langle [\mathbf{X}(\xi, \eta) - \mu][\mathbf{X}(\xi + \tau, \eta + \psi) - \mu]^T \rangle, \quad (5)$$

where $\langle \dots \rangle$ denotes expectation under the appropriate joint probability distribution, μ is the mean vector and the superscript T means transposition. Every covariance matrix is characterized by the shift pair (τ, ψ) , where τ and ψ are increments in the ξ and η coordinates.

From eq. (2) we can easily derive a relation between the data covariance matrix \mathbf{C}_x at a certain lag, the source covariance matrix \mathbf{C}_s at the same lag, the mixing matrix \mathbf{H} , and the noise covariance matrix \mathbf{C}_n :

$$\mathbf{C}_x(\tau, \psi) = \mathbf{H}\mathbf{C}_s(\tau, \psi)\mathbf{H}^T + \mathbf{C}_n(\tau, \psi). \quad (6)$$

This relation allows us to estimate the mixing operator \mathbf{H} from the covariance matrix \mathbf{C}_x of the data. Note that it implicitly assumes that the source and the noise processes are stationary. This is true all across the sky for the CMB, but only within small sky patches for the foregrounds. For this reason, it is convenient to section the sky into patches within which foregrounds have approximately uniform properties, and apply the method to individual patches. In this way the only remaining issue is the non-stationarity of noise, depending on the particular scanning strategy adopted, which we do not consider in this work.

If the noise process can be assumed to be signal-independent, white and zero-mean, for $(\tau, \psi) = (0, 0)$ \mathbf{C}_n is a diagonal matrix whose elements are the noise variances in the frequency channels of the instrument, while for $(\tau, \psi) \neq (0, 0)$ \mathbf{C}_n is the null $M \times M$ matrix. Anyway, if \mathbf{C}_n deviates significantly from this ideal model, various methods are available to estimate the noise covariance function: for example it can be empirically determined using noise maps from Monte Carlo simulations.

Once we have a model for \mathbf{C}_n , we only have to calculate \mathbf{C}_x for a large enough number of nonzero shift pairs (τ, ψ) to estimate both \mathbf{H} and \mathbf{C}_s . In practice, however, we need to parameterize the mixing matrix to reduce the number of unknowns. We note that for the scaling ambiguity, we can normalize our mixing matrix to have all elements of a reference row equal to 1.

The main product of CCA is then an estimate of the mixing matrix. Hence this can be considered a “model learning” algorithm. Once the mixing matrix have been recovered, source separation can be performed with traditional non-blind methods, such as WF or MEM, or other Bayesian inversion techniques.

2.1 Parameterization of the mixing matrix

To choose a suitable parameterization for \mathbf{H} we use the fact that its elements are proportional to the spectra of astrophysical sources, of which we have some knowledge coming from the theory or from complementary observations. The main diffuse components present in the PLANCK channels are, in addition to the CMB, the Galactic dust, synchrotron and free-free emissions. The frequency dependencies of the CMB and of the free-free are known; in terms of the antenna temperature we have:

$$T_{A,\text{CMB}}(\nu) \propto \frac{(h\nu/kT_{\text{CMB}})^2 \exp(h\nu/kT_{\text{CMB}})}{(\exp(h\nu/kT_{\text{CMB}}) - 1)^2}, \quad (7)$$

$$T_{A,\text{ff}}(\nu) \propto (\nu)^{-2.14}, \quad (8)$$

where h is the Planck constant, k the Boltzmann constant, $T_{\text{CMB}} = 2.726$ K. Conversely, the frequency scalings of synchrotron and dust are not known a priori. The simplest model compatible with observations involves only one parameter for each source, the spectral index β_s or the emissivity index β_d , respectively:

$$T_{A,\text{synch}}(\nu) \propto \nu^{-\beta_s}, \quad (9)$$

$$T_{A,\text{dust}}(\nu) \propto \frac{\nu^{\beta_d+1}}{\exp(h\nu/kT_{\text{dust}}) - 1}. \quad (10)$$

The mixing matrix accounting for all these sources is then of four columns and of as many rows as the number of channels. We are able to parameterize the matrix \mathbf{H} by exploiting eqs. (3) or (4). The integrals in eq. (3) can be evaluated with f_c replaced by one of the emission spectra in eqs. (7)-(10).

Under the above assumptions, we only have two free parameters, β_s and β_d . When we work with the high frequency PLANCK channels, synchrotron and free-free can be neglected, so the mixing matrix has two columns, one for the CMB and one for the dust, and only one parameter, β_d .

Since β_s and β_d vary across the sky, we will apply the CCA to sky patches small enough for these indices can be assumed to be approximately constant, as we specify in Section 5.

3 IMPLEMENTATION

3.1 Computation of the data covariance matrix

The data covariance matrix defined by eq. (5) is the fundamental tool used to identify the mixing operator. If our data are sampled in P pixels, labelled with coordinates (ξ, η) , we can compute an estimate of \mathbf{C}_x as:

$$\hat{\mathbf{C}}_x(\tau, \psi) = \frac{1}{P} \sum_{\xi, \eta} [\mathbf{x}(\xi, \eta) - \mu_x] \cdot [\mathbf{x}(\xi + \tau, \eta + \psi) - \mu_x]^T. \quad (11)$$

The shift pair (τ, ψ) defines a vector that links each pixel to a shifted one. In the case of a uniformly sampled rectangular sky patch we have a very easy way to define the shift pairs (τ, ψ) . We choose (ξ, η) as cartesian coordinates whose axes are parallel to the sides of the rectangle, and define a collection of N_p shifts, each of p pixels, labelled by an index n ($n = 0, 1, \dots, N_p - 1$): $\{\tau_n = n p \mathbf{u}_\xi\}$ and $\{\psi_n = n p \mathbf{u}_\eta\}$. From all the combinations of τ_n and ψ_n we get $N_p \times N_p$ shift pairs.

The data we are working with are very different from this simple case: they are patches extracted from Healpix (Górski et al. 2005) all sky maps, so they are sampled in a sphere rather than in a plane and also the grid is not regular. We note that even in the simplest case the selected region is not exactly rectangular because of the diamond shape of pixels and of the surface curvature.

To apply the method we need to map the selected patch into a geometrically identical one, shifted by (τ, ψ) . This can be done only in an approximate way with the Healpix pixelization, and is easier in the equatorial region. In the present application we study Galactic foregrounds where they are more intense, i.e. at not too high Galactic latitudes. We therefore use Galactic coordinates and refer to the grid defined by Galactic parallels and meridians to calculate shifts.

With the Healpix ring ordering scheme, pixels with subsequent indices are subsequent in longitude, so that, for any integer p , a set of pixels $i_{\min} \leq i \leq i_{\max}$ simply map into the set

$i_{\min} + p \leq i \leq i_{\max} + p$, shifted by p pixels in the longitudinal direction. The shift in latitude is trickier. We proceeded associating to each pixel the shifted one closest to having the same longitude and the latitude increased by $\Delta b = p \cdot ds$, where ds is the mean pixel size. Clearly, in this case Δb is not exactly equal for all shifted pixels. However, our shifts are rather small (see below), so that, if we are not too close to the Galactic poles, the approximation is sufficiently good.

To choose convenient values for the number of shifts N_p and the step p , we should care both about efficiency and conditioning. It is obvious that, if N_p is large, the method becomes computationally demanding. On the other hand, a too small N_p can make the problem ill conditioned, thus leading to a lack of convergence. The step p should be chosen in order to avoid both redundancy (if p is small, some of the covariance matrices are nearly equal) and degeneracy (if p is too large, some covariance matrices vanish). In practice, the choice can be made empirically, for any p , by increasing N_p progressively until convergence is reached.

3.2 The minimization procedure

To solve eq. (6) and estimate the parameters that identify the mixing matrix and the source covariance matrices, we minimize the residual between the theoretical quantities based on the proposed solution and the corresponding quantities evaluated empirically from the available data. Our solution is given by:

$$(\Gamma, \Sigma(:, :)) = \underset{\tau, \psi}{\operatorname{argmin}} \sum \left\| \mathbf{H}(\Gamma) \mathbf{C}_s[\Sigma(\tau, \psi)] \mathbf{H}^T(\Gamma) - \hat{\mathbf{C}}_x(\tau, \psi) + \mathbf{C}_n(\tau, \psi) \right\|, \quad (12)$$

where Γ is the vector of all parameters defining \mathbf{H} , and $\Sigma(:, :)$ is the vector containing all the unknown elements of the matrices \mathbf{C}_s for every shift pair.

To perform the minimization, we used simulated annealing (SA, Aarts & Korst, 1989), which exploits an analogy between the way in which a metal cools and freezes into a minimum energy crystalline structure and the search for a minimum in a more general system.

The major advantage of SA over other methods is its ability to avoid becoming trapped at local minima, which can be very nasty in our case. The algorithm employs a random search which not only accepts changes that decrease the objective function f , but also some changes that increase it. The latter are accepted with a probability:

$$p = \exp(-\delta f/T), \quad (13)$$

where δf is an increment in f and T is a control parameter, known as the system “temperature”.

Avoidance of local minima is anyway dependent on the “annealing schedule”: the choice of the initial temperature, how many iterations are performed at each temperature, and how much the temperature is decreased at each step as cooling proceeds.

4 TESTS ON SIMULATED SKIES

For this set of tests we used the specifications of the PLANCK mission (see Table 1). The simulated sky contains: a) synchrotron emission as modelled by Giardino et al. (2002), allowing for a spatially varying spectral index; b) thermal dust emission (Finkbeiner et al. 1999), with dust at two temperatures and two emissivity indices;

Table 1. PLANCK specifications. We assume spatially uniform Gaussian noise at the mean level expected for the nominal mission (14 months)

Center frequency (GHz)	30	44	70	100	143	217	353	545	857
Angular resolution (arcmin)	33	24	14	9.5	7.1	5.0	5.0	5.0	5.0
Rms pixel noise ΔT (μK thermodynamic)	5.5	7.4	12.8	6.8	6.0	13.1	40.1	401	18291

c) free-free traced by the H_α emission (Dickinson et al. 2003) and corrected for dust absorption with the 100 μm maps from Schlegel et al. (1998); d) a CMB Gaussian realization corresponding to the best fit WMAP theoretical power spectrum from first year data. We produced 100 sets of Monte Carlo simulated maps in the PLANCK channels, with different realizations of the CMB and of Gaussian noise.

To test the CCA ability to recover the spectral parameters of foregrounds, we used the PLANCK channels from 30 to 143 GHz. The resolution of all the maps had to be degraded to that of the 30 GHz channel ($33'$). To test the performances achievable with the full PLANCK resolution of $5'$, we repeated the analysis with the high frequency channels from 217 to 545 GHz, where the sources to account for are only CMB and dust.

The noise maps we initially added to each channel were Gaussian (with the rms levels reported in Table1) and uncorrelated: in this case, the only noise term in eq. (6) is $\mathbf{C}_n(0, 0)$, which is a diagonal matrix whose elements are the noise variances for each channel. The smoothing process applied to degrade the channels to the 30 GHz resolution not only changes the noise variances, but also introduces noise correlation, so in principle the terms $\mathbf{C}_n(\tau, \psi)$ do not vanish for $(\tau, \psi) \neq (0, 0)$. Nevertheless, we carried out our tests assuming uncorrelated Gaussian noise: we then consider only the diagonal matrix $\mathbf{C}_n(0, 0)$, whose elements are the variances measured after smoothing each noise map to the $33'$ resolution. This approximation is not the best we could do in dealing with noise, but it was purposely adopted to investigate the effect of errors on noise modelling.

4.1 The low frequency channels (LF) set

The LF set includes 5 PLANCK channels, centered at 30, 44, 70, 100, and 143 GHz. Since we have 4 sources (CMB, synchrotron, free-free, and thermal dust) the mixing matrix has 4 columns and we want to recover the synchrotron and the dust spectral indices. Since all the maps have been degraded to a resolution of $33'$, we operate with the Healpix parameter NSIDE=512, corresponding to a pixel size of about $7'$.

The number of shifts allowing a good conditioning of the problem is found to be $N_p = 5$. The value of N_p and the pixel size constrain the amplitude of the shifts that can be used to calculate the covariance matrices: the minimum shift must correspond to one pixel ($\sim 0.1^\circ$); the maximum one cannot generally exceed 1° to ensure that all covariance matrices are non-null. We chose $p = 4$, which corresponds roughly to our beam size.

There is a second effect of the resolution: to have sufficient statistics, the number of pixels per patch has to be at least $\simeq 10^5$. With the adopted pixel size, this corresponds to a patch area of 1500 deg^2 , which is not optimal for the reconstruction of the spectral indices that may vary widely with the position. In the synchrotron template we use here (Giardino et al. 2002), 10% variations occur on scales of about 10 degrees.

We used patches of $(\Delta l, \Delta b) = (50^\circ, 30^\circ)$ for the lowest

latitudes and increased the longitudinal dimension for higher latitudes to roughly preserve the patch area. We sectioned the sky with patches centered at longitudes $l_c = \{0^\circ, 40^\circ, 80^\circ, \dots, 320^\circ\}$ and increasing latitudes. In total we analyzed the $\sim 80\%$ of the sky with $|b| < 55^\circ$.

From the first tests we learned that to get a good spectral index reconstruction we need a broad frequency range. This can be achieved by taking into account additional information from other surveys. To this end, we included in our analysis the 857 GHz PLANCK map and the Haslam et al. (1982) 408 MHz map, taken as dust and synchrotron templates, setting to 0 all the elements of the mixing matrix except the synchrotron one at 408 MHz, and the dust one at 857 GHz.

4.2 The high frequency channels (HF) set

In the PLANCK 217, 353 and 545 GHz channels we can neglect the synchrotron and free-free emissions, so that we are left with CMB and dust, and the only parameter to recover is the dust emissivity index β_d . These channels allow us to work at the best PLANCK resolution: the beam is of $5'$, so we can use NSIDE=2048, corresponding to a pixel size of about $1'.7$. We dissected the sky into patches of size $(\Delta l, \Delta b) = (20^\circ, 20^\circ)$, centered at longitudes $l_c = \{0^\circ, 20^\circ, 40^\circ, \dots, 340^\circ\}$ and latitudes $b_c = \{0^\circ, \pm 10^\circ, \pm 20^\circ, \pm 40^\circ, \pm 60^\circ\}$. In total, we then analyzed $\sim 85\%$ of the sky.

In this case, we did not need to include other channels to help reconstructing the mixing matrix. We used a shift step $p = 5$, corresponding to an angular size of 0.14° , and $N_p = 3$.

5 ESTIMATION OF THE MIXING MATRIX

5.1 Error estimates

Since, on purpose, the parameters to be determined do not directly reflect those defining the sky model, the errors on our estimates cannot be simply derived comparing our results with the “true” values, simply because the latter in general do not exist. In particular, the synchrotron spectral index is varying in the sky, and the dust emission is modeled by a two-component spectrum, so they need to be treated as we describe below.

The output of our method is the estimated mixing matrix normalized at a reference frequency ν_0 . The elements of the mixing matrix corresponding to synchrotron and dust at frequency ν_d are:

$$h_{\text{out}}(\text{syn}, \nu_d) = \left(\frac{\nu_d}{\nu_0}\right)^{-\beta_s}, \quad (14)$$

$$h_{\text{out}}(\text{dust}, \nu_d) = \left(\frac{\nu_d}{\nu_0}\right)^{\beta_d+1} \frac{\exp(h\nu_0/kT_{\text{dust}}) - 1}{\exp(h\nu_d/kT_{\text{dust}}) - 1}, \quad (15)$$

which were derived from eqs. (3), (9) and (10) by assuming $b_d(\nu) = \delta(\nu - \nu_d)$. These quantities correspond to the mean ratios of synchrotron and dust intensities at frequencies ν_0 and ν_d , within the considered patch in the simulated sky:

$$h_{\text{in}}(\text{syn}, \nu_d) = \left(\frac{\nu_d}{\nu_0}\right)^{-\bar{\beta}_s}, \quad (16)$$

$$h_{\text{in}}(\text{dust}, \nu_d) = \left(\frac{\nu_d}{\nu_0}\right)^{\bar{\beta}_d+1} \frac{\exp(h\nu_0/kT_{\text{dust}}) - 1}{\exp(h\nu_d/kT_{\text{dust}}) - 1}. \quad (17)$$

The ‘‘observed’’ indices $\bar{\beta}_s$ and $\bar{\beta}_d$ are now directly comparable with the derived indices β_s and β_d . We then define our errors as:

$$\Delta\beta_s = \left| \frac{\log(h_{\text{out}}(\text{syn}, \nu_d)/h_{\text{in}}(\text{syn}, \nu_d))}{\log(\nu_d/\nu_0)} \right|, \quad (18)$$

$$\Delta\beta_d = \left| \frac{\log(h_{\text{out}}(\text{dust}, \nu_d)/h_{\text{in}}(\text{dust}, \nu_d))}{\log(\nu_d/\nu_0)} \right|. \quad (19)$$

5.2 Results for the mixing matrix identification

Figure 1 refers to the analysis of the LF set and shows the mean values of $\Delta\beta_s$ and $\Delta\beta_d$, over 100 simulations of the sky, as a function of longitude for latitudes $b = \{0^\circ, \pm 10^\circ, \pm 15^\circ\}$. The error bars, generally very small and barely visible in the figure, are the standard deviations of $\Delta\beta_s$ and $\Delta\beta_d$ from the mean. Their small values imply that the errors in the spectral index recovery are mainly systematic; for both spectral indices, part of the systematic error comes from the fact that the models we assume for the analysis differ from those defining the sky model. We clearly have problems with the estimation of the synchrotron spectral index, while the errors on β_d are generally small.

We have checked that this effect is due to confusion between synchrotron and free-free. The free-free emission is highly concentrated on the Galactic plane but depresses the mean spectral index of the combined emission over entire patches, thus biasing the estimate of the synchrotron spectral index. A better recovery of the latter would be possible with high spatial resolution maps, so that we have a sufficient number of pixels within a much smaller range of Galactic latitudes.

With the angular resolution adopted here, this effect can be minimized by cutting out a strip of a few degrees around the Galactic plane. The situation is substantially better even with a cut of $\pm 1^\circ$ around the Galactic equator, and improves further if we enlarge the cut to $\pm 3^\circ$ (Fig. 2). All the tests described below are performed by applying this cut, even though its effects are modest when working with the HF channels.

Figure 3 summarizes the results obtained over all the analyzed region of the sky with both the LF and HF sets. We computed the mean errors on synchrotron and dust indices over 100 Monte Carlo iterations for each patch, and the mean and standard deviation of errors obtained for patches at the same latitude. The bars are the standard deviations around the mean over longitudes.

For the LF set, while the dust index is always reconstructed with an error of $\simeq 0.05$, the error on the synchrotron spectral index increases with latitude. This is due to the fact that the substantial spatial variability of the synchrotron spectral index, implied by the Giardino et al. (2002) model, is increasingly difficult to recover as the synchrotron signal weakens with increasing Galactic latitude.

Thanks to the higher angular resolution of the HF set and to the lack of other relevant diffuse components besides CMB and dust in this frequency range, the CCA allows us to reconstruct the dust spectral index with an error ~ 0.03 over the full latitude range analyzed.

6 ESTIMATION OF ERRORS IN THE CMB POWER SPECTRUM

The CCA procedure can be viewed as the first step (learning) in component separation. In a further step, the mixing matrix estimated by this approach can be input to non-blind separation techniques. The performances of non-blind techniques are normally evaluated as functions of the system noise, assuming perfectly known mixing matrices. In this section, we estimate the uncertainties on the CMB power spectrum induced by the errors in the mixing matrix resulting from our simulations. Since at the moment the optimal component separation method exploiting the information recovered by CCA has still to be developed, we try to estimate the errors in the CMB spectrum under conservative hypotheses. Clearly, the errors will depend on the approach adopted to separate the individual components. We investigated the general case where component separation is performed by a generic linear filter and, in particular, by a Wiener filter, and a pseudo-inverse reconstruction. The data model we assume provides a space-invariant mixing matrix \mathbf{H} , obtained with spectral indices β_s and β_d as defined in Section 5.1. To evaluate the errors caused by an approximated estimate of the mixing matrix, we assumed the estimated matrix, $\hat{\mathbf{H}}$, to be generated by a distribution of the spectral indices such as the one described in the above sections. Following a theoretical derivation, the errors are evaluated in terms of quantities that are known for our simulation, thus allowing the estimation to be made without actually separating the components.

Given the mixing matrix, one way to solve eq. (2) is to work in a conjugate space. If we work with sky patches that are small enough for curvature effects can be neglected, the correct basis functions are the Fourier complex exponentials; on the whole celestial sphere, the good basis functions are the spherical harmonics; finally, in the presence of an incomplete sky coverage, pixelization, and position-dependent noise, the basis functions can be calculated according to Tegmark (1996). For simplicity, we are going to derive the equations in spherical harmonics.

In the harmonic space, the problem stated in eq. (2) simply becomes:

$$\mathbf{x}_{lm} = \mathbf{H}\mathbf{s}_{lm} + \mathbf{n}_{lm}, \quad (20)$$

where the vectors \mathbf{x}_{lm} , \mathbf{s}_{lm} , and \mathbf{n}_{lm} contain the harmonic coefficients of channels, sources and instrumental noise, respectively. Using a linear approach to component separation, an estimate of the vector \mathbf{s}_{lm} , say $\hat{\mathbf{s}}_{lm}$, can be obtained as:

$$\hat{\mathbf{s}}_{lm} = \mathbf{W}_{\hat{\mathbf{H}}}^{(l)} \mathbf{x}_{lm}, \quad (21)$$

where $\mathbf{W}_{\hat{\mathbf{H}}}^{(l)}$, referred to as the *reconstruction matrix*, is some matrix-valued function depending on the estimate $\hat{\mathbf{H}}$ of the mixing matrix. The random matrix $\hat{\mathbf{H}}$ is estimated with the method proposed in this paper, and is a function of the estimated spectral indices. Following Tegmark & Efstathiou (1996) and Bouchet & Gispert (1999), the estimation error on the source spectra, in matrix notation, can be expressed as:

$$\Delta\mathbf{C}_{\hat{\mathbf{H}}}^{(l)} = \frac{1}{2l+1} \sum_{m=-l}^l \langle (\hat{\mathbf{s}}_{lm} - \mathbf{s}_{lm})(\hat{\mathbf{s}}_{lm} - \mathbf{s}_{lm})^\dagger \rangle, \quad (22)$$

where $\langle \dots \rangle$ indicates expectation and \dagger indicates conjugate transposition. By using eqs. (20) and (21), after a straightforward calculation, we have:

$$\Delta\mathbf{C}_{\hat{\mathbf{H}}}^{(l)} = (\mathbf{W}_{\hat{\mathbf{H}}}^{(l)}\mathbf{H} - \mathbf{I})\mathbf{C}_s^{(l)}(\mathbf{W}_{\hat{\mathbf{H}}}^{(l)}\mathbf{H} - \mathbf{I})^\dagger +$$

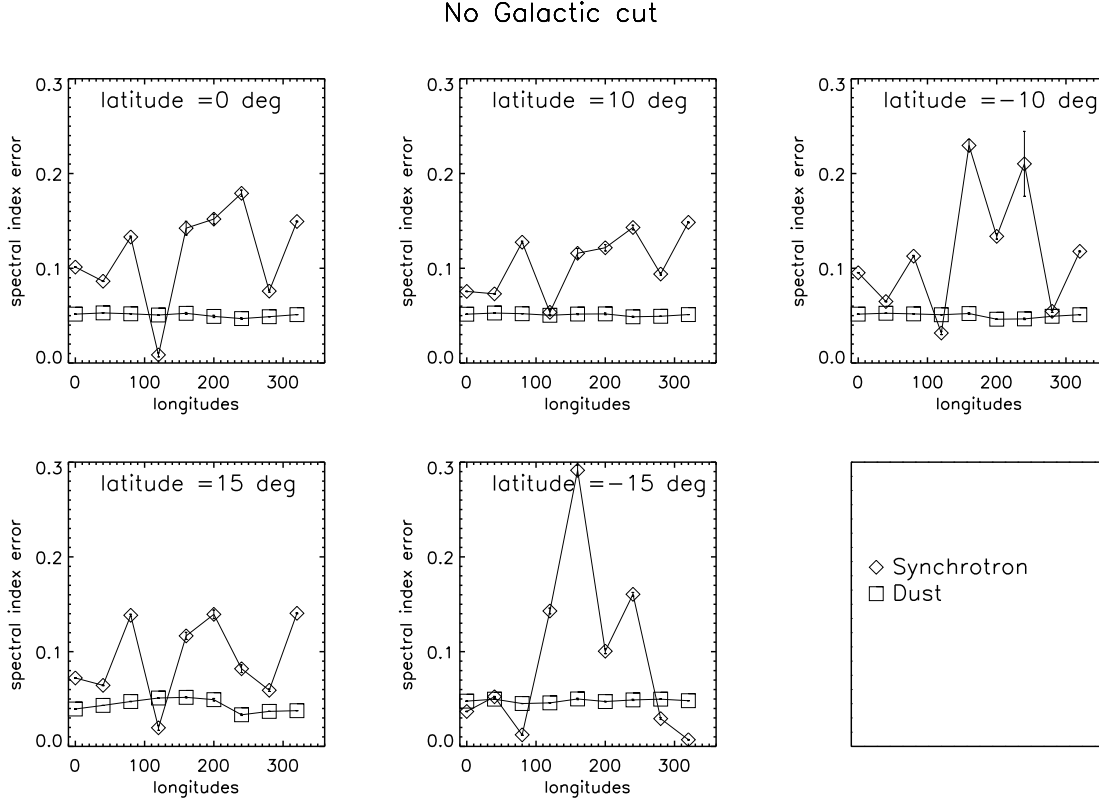


Figure 1. Absolute errors in the spectral index reconstruction for the LF channels without cuts

$$+ \mathbf{W}_H^{(l)} \mathbf{C}_n^{(l)} (\mathbf{W}_H^{(l)})^\dagger, \quad (23)$$

where \mathbf{I} is the identity matrix, and \mathbf{C}_s and \mathbf{C}_n are, respectively, the source and the noise power spectra.

Eq. (23) can be simplified by assuming that the source and the noise processes are mutually uncorrelated: in this case \mathbf{C}_s , \mathbf{C}_n and $\Delta \mathbf{C}_H^{(l)}$ are diagonal matrices. If we define:

$$C_s^{(l)}(i) \equiv \mathbf{C}_s^{(l)}(i, i), \quad (24)$$

$$C_n^{(l)}(i) \equiv \mathbf{C}_n^{(l)}(i, i), \quad (25)$$

the estimation error on the i -th source is:

$$\begin{aligned} \Delta C_H^{(l)}(i) &\equiv \Delta \mathbf{C}_H^{(l)}(i, i) = \sum_{j=1}^N |(\mathbf{W}_H^{(l)} \mathbf{H} - \mathbf{I})_{ij}|^2 C_s^{(l)}(j) + \\ &+ \sum_{j=1}^M |W_H^{(l)}(i, j)|^2 C_n^{(l)}(j), \end{aligned} \quad (26)$$

where N is the number of sources and M the number of channels. The error $\Delta C_H^{(l)}(i)$ refers to the frequency at which the mixing matrix has all its elements equal to 1. Eq. (26) highlights how the different terms affect the estimation error: the first term accounts for the contamination due to the other sources, while the second one accounts for the effect of the instrumental noise. Note that in the first term of eq. (26) there is the product of the reconstruction matrix $\mathbf{W}_H^{(l)}$, depending on the estimated mixing matrix $\hat{\mathbf{H}}$, with the true mixing matrix \mathbf{H} . As we will see, this term is minimum when $\hat{\mathbf{H}} = \mathbf{H}$ and increases as the estimated mixing matrix differs from the true one. From eq. (26), we can approximately evaluate the

error on the spectrum of any component, provided that the source and noise spectra are known, without explicitly reconstructing that component.

Tegmark & Efstathiou (1996) and Bouchet & Gispert (1999) performed an accurate analysis of eqs. (23) and (26) when the reconstruction matrix is a Wiener filter:

$$\mathbf{W}_H^{(l)} = \mathbf{C}_s^{(l)} \mathbf{H}^T [\mathbf{H} \mathbf{C}_s^{(l)} \mathbf{H}^T + \mathbf{C}_n^{(l)}]^{-1}, \quad (27)$$

where the mixing matrix is assumed as perfectly known, that is, $\hat{\mathbf{H}} = \mathbf{H}$. They found that, although the Wiener filter reduces the error due to instrumental noise, the contamination error due to the other sources is always present, even if the actual matrix \mathbf{H} is known. Moreover, the spectra estimated from the sources, as given by eq. (21), are biased. The following equation can be easily derived:

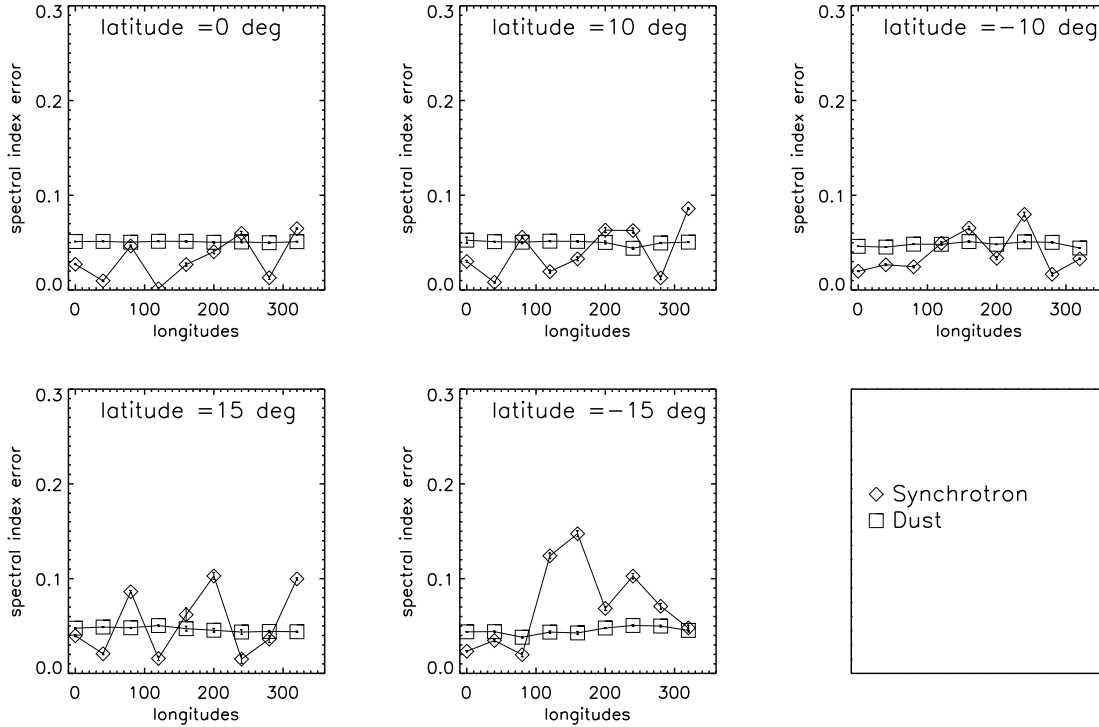
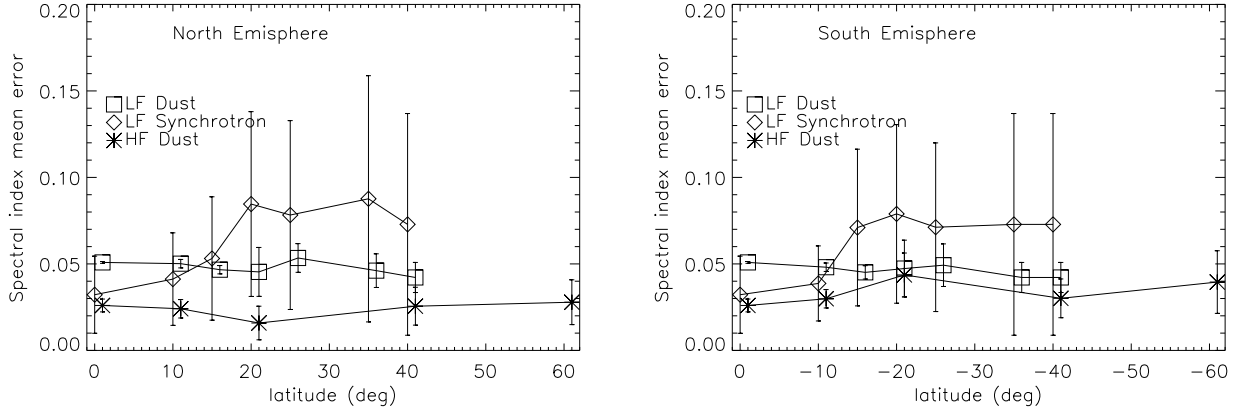
$$\mathbf{C}_s^{(l)} = \frac{1}{2l+1} \sum_{m=-l}^l \langle \hat{s}_{lm} \hat{s}_{lm}^\dagger \rangle = \mathbf{W}_H^{(l)} \mathbf{H} \mathbf{C}_s^{(l)}. \quad (28)$$

Bouchet & Gispert (1999) proposed to use a quality factor derived from the quantity $\mathbf{W}_H^{(l)} \mathbf{H}$ in order to correct the estimated CMB power spectrum.

If we reconstruct the sources by the following pseudo-inverse filter:

$$\mathbf{W}_H = (\mathbf{H}^T \mathbf{H})^{-1} \mathbf{H}^T, \quad (29)$$

we have $\mathbf{W}_H \mathbf{H} = \mathbf{I}$. Then, eq. (23) tells us that the estimation error is only due to instrumental noise. Moreover, the mean of the estimated power spectrum is:

Galactic cut = $[-3.0, +3.0]$ deg

Figure 2. Absolute errors in the spectral index reconstruction for LF channels cutting out the Galactic plane region $|b| \leq 3^\circ$

Figure 3. Mean absolute spectral index errors versus Galactic latitude for the analysis of LF and HF channels with the Galactic cut of $\pm 3^\circ$

$$\mathbf{C}_s^{(l)} = \mathbf{C}_s^{(l)} + \mathbf{W}_H \mathbf{C}_n^{(l)} (\mathbf{W}_H)^\dagger. \quad (30)$$

It is apparent that this estimate is unbiased, but for large multipoles the noise term becomes dominant on the reconstructed source spectrum. When the noise spectrum is known, as in the case of the PLANCK experiment, eq. (30) can be used to correct the estimated spectra.

To evaluate the uncertainties on the estimated CMB spectrum when the mixing matrix is not known exactly, we used a Monte Carlo approach: we generated 100 mixing matrices $\hat{\mathbf{H}}$ drawn from

the probability distribution for the spectral indices described below. For each matrix we computed the $\Delta C_{\hat{\mathbf{H}}}^{(l)}$ (cmb) from eq. (26). For the LF set, these errors have been evaluated at the reference frequency of 100 GHz using four sources (CMB, synchrotron, dust and free-free) and five channels (30, 44, 70, 100, 143 GHz). For the HF set we used two sources (CMB and dust) and three channels (217, 353, 545 GHz), with the reference frequency at 217 GHz. For each channel set, we used the all-sky power spectra of the reference

source templates as the input spectra $C_s^{(l)}(i)$. The $C_n^{(l)}(i)$ for each channel have been calculated as:

$$C_n^{(l)}(i) = 4\pi\sigma_i^2/N_i, \quad (31)$$

where N_i is the number of pixels, and the rms pixel noise values σ_i have been taken from Table 1.

As we have been working with sky patches, we should perform Monte Carlo simulations patch by patch, using the appropriate basis, and then combine the information over the whole sky. However, since we only want to get an indicative amplitude for $\Delta C_{\hat{H}}^{(l)}(cmb)$, we only performed our trials on a single set of all-sky simulations, decomposed into spherical harmonics. On the other hand, since an adequate strategy to combine the results obtained on patches to achieve a coordinated all-sky component separation has yet to be developed, we will confine ourselves to the multipole range constrained by the patch size.

For each iteration of our Monte Carlo simulations, we generated the mixing matrix from synchrotron and dust spectral indices that are Gaussian-distributed around their true values $\bar{\beta}_s$ and $\bar{\beta}_d$. In particular, we used standard deviations of 0.1 and 0.05, respectively, for the distributions of synchrotron and dust indices in the LF channels, and a standard deviation of 0.03 for the dust index in the HF channels. These values are upper limits to the ones shown in Fig. 3. We then exploited eq. (26) to compute the error on the CMB power spectrum for both the Wiener filter and the pseudo-inverse filter. From our Monte Carlo simulations, we computed the average value of $\Delta C_{\hat{H}}^{(l)}(cmb)$, which is the total error on the CMB power spectrum estimation. We also estimated the standard deviation $\sigma_{\Delta C}$ of the random variable:

$$\Delta C_{\hat{H}}^{(l)}(cmb) - \Delta C_H^{(l)}(cmb), \quad (32)$$

where $\Delta C_H^{(l)}(cmb)$ is obtained for $\hat{\mathbf{H}} = \mathbf{H}$, and assumed it as the error on the CMB spectrum due to the estimation of the mixing matrix.

The results are shown in Figs. 4 and 5. In Fig. 4 we show the errors for both the Wiener filter and the pseudo-inverse filter from the LF channel data, as functions of the multipole l , together with the original CMB power spectrum. Figure 5 displays the corresponding results for the HF channels. All the errors are computed without correction for the noise contribution; cosmic variance is not included. Note that the Wiener filters are more accurate, but the differences with the pseudo-inverse solutions decrease once corrections for noise are applied. This is particularly true for the HF set, where the noise level is higher. The total error on the CMB power spectrum $\Delta C_{\hat{H}}^{(l)}(cmb)$ turns out to be of the order of 1% for both the channels sets, and decreases from lower to higher multipoles. In both cases the contribution of the errors in the estimation of the mixing matrix is subdominant.

7 CONCLUSIONS

The tests described here demonstrate that the Correlated Component Analysis (CCA) method (Bedini et al. 2005), applied to simulated data with PLANCK specifications, is a promising tool to estimate the mixing matrix parameterizing the frequency scaling of different astrophysical signals in cosmic microwave background (CMB) observations. For the low frequency PLANCK channels, from 30 to 143 GHz, and with the angular resolution of $33'$, the most accurate estimates are obtained in the latitude range $[-30^\circ, +30^\circ]$, where the foregrounds we aim to recover are relatively strong.

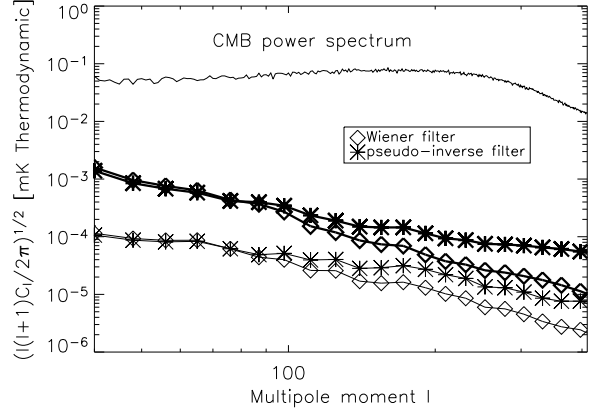


Figure 4. Estimated errors on the CMB power spectrum at 100 GHz for the LF set, for Wiener filter and pseudo-inverse filter. For each filter, the thicker (upper) line shows the total error, the lighter (lower) one is the contribution due to errors in the mixing matrix estimation.

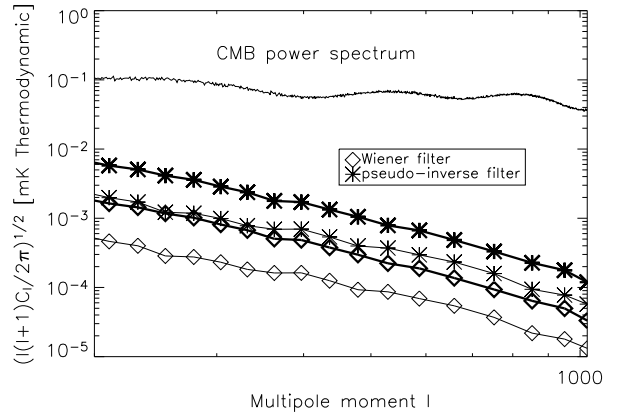


Figure 5. Same as in Fig. 4, but for the HF set, at the reference frequency of 217 GHz.

However, the strong concentration of intense free-free emission in a narrow strip (a few degrees wide) around the Galactic equator introduces a large gradient of the global spectral index of Galactic radio emission (synchrotron plus free-free) that prevents an accurate recovery of the synchrotron spectral index with the low resolution of the LF channels. The problem is cured cutting out the strip at $|b| < 3^\circ$. Having done that, both the synchrotron and the dust spectral index are recovered with a mean absolute error of 0.05. At higher latitudes, the mean error on the synchrotron index increases to 0.08, while that on the dust index is unchanged.

The situation is even better with the high frequency PLANCK channels, from 217 to 545 GHz, thanks to the better spatial resolution ($5'$) and to the fact that the only relevant foreground, at least on intermediate angular scales, is Galactic dust.

We have shown that, exploiting non-optimized component separation techniques, such as Wiener filter and pseudo-inverse filter, such errors allow us to estimate the CMB power spectrum with an uncertainty of the order of 1% on the angular scales constrained by our patch size.

We conclude that the CCA can be a promising independent way to probe the spectral behaviour of the main foregrounds affecting the CMB. This second order statistical approach may allow us to increase our knowledge on foregrounds and to perform component separation with traditional non-blind methods with a minimum number of priors.

ACKNOWLEDGMENTS

We gratefully acknowledge useful comments and suggestions from the anonymous referee. Work supported in part by MIUR and ASI.

REFERENCES

- Aarts E., Korst J., 1989, *Simulated Annealing and Boltzmann Machines*, New York, Wiley
- Amari S., Chichocki A., 1998, *proc. IEEE* 86, 2026
- Baccigalupi C. et al., 2000, *MNRAS*, 318, 769
- Baccigalupi C., Perrotta F., de Zotti G., Smoot G. F., Burigana C., Maino D., Bedini L., Salerno E., 2004, *MNRAS*, 354, 55
- Barreiro R. B., Hobson M. P., Banday A. J., Lasenby A. N., Stolyarov V., Vielva P., Górski K. M., 2004, *MNRAS*, 351, 515
- Bedini L., Herranz D., Salerno E., Baccigalupi C., Kuruoğlu E.E., Tonazzini A., 2005, *EURASIP Journal on Applied Signal Processing*, 15, 2400
- Belouchrani A., Abed-Meraim K., Cardoso J.-F., Moulines E., 1997, *IEEE Trans. on signal Processing*, 45, 434
- Bennett C. L. et al., 2003a, *ApJS*, 148, 1
- Bennett C. L. et al., 2003b, *ApJS*, 148, 97
- Bouchet F.R., Prunet S., Sethi S.K., 1999, *MNRAS*, 302,663
- de Zotti G., Toffolatti L., Argüeso F., Davies R.D., Mazzotta P., Partridge R.B., Smoot G.F., Vittorio N., 1999, *AIPC*, 476, 204
- Dickinson C., Davies R.D., & Davis R.J., 2003, *MNRAS*, 341 369
- Eriksen H.K., Dickinson C., Lawrence C.R., Baccigalupi C., Banday A.J., Górski K.M., Hansen F.K., Lilje P.B., Pierpaoli E., Seiffert M.D., Smith K.M. & Vanderlinde K., 2006, *ApJ*, 641, 665
- Finkbeiner D.P., Davies M., Schelegel D.J., 1999, *ApJ* 524, 867
- Finkbeiner D.P., 2003 *ApJS*, 146, 407
- Giardino G. et al., 2002, *A&A*, 387, 82
- Górski K.M., Hivon E., Banday A.J., Wandelt B.D., Hansen F.K., Reinecke M., Bartelmann M., 2005, *ApJ* 622, 759
- Haffner L.M., Reynolds R.J., Tufte S.L., 1999, *ApJ*, 523, 233
- Haslam C. G. T. et al., 1982, *A&A S* 47,1
- Hivon E., Górski K.M., Netterfield C.B., Crill B.P., Prunet S., & Hansen F., 2002, *ApJ*, 567,2
- Hyvärinen A. 1999, *IEEE Signal Processing Lett.* 6, 145
- Hobson M.P., Jones A.W., Lasenby A.N., Bouchet F., 1998, *MNRAS*, 300,1
- Lamarre J. M. et al., 2003, *NewAR*, 47, 1017
- Maino D. et al., 2002, *MNRAS*, 334, 53
- Maino D., Banday A. J., Baccigalupi C., Perrotta F., Górski K. M., 2003, *MNRAS*, 344, 544
- Maisinger K., Hobson M. P., Lasenby A. N., 2004, *MNRAS*, 347, 339
- Mandolesi N., Morgante G., Villa F., 2003, *SPIE*, 4850, 722
- Patanchon G., Cardoso J.-F., Delabrouille J., Vielva P., 2005, *MNRAS*, 364, 1185
- Schlegel D.J., Finkbeiner D.P., Davies M., 1998, *ApJ* 500, 525
- Spergel D.N. et al., 2006, submitted to *ApJS* (astro-ph/0603449)
- Stivoli S., Baccigalupi C., Maino D., Stompor R., 2006, submitted to *MNRAS* (astro-ph/0505381)
- Stolyarov V., Hobson M. P., Lasenby A. N., Barreiro R. B., 2005, *MNRAS*, 357, 145
- Tauber J.A., 2004, *AdSpR*, 34, 491
- Tegmark M., 1996, *MNRAS* 280,299
- Tegmark M., Efstathiou G., 1996, *MNRAS* 281, 1297